

## Cold Air Incursions over Subtropical South America: Mean Structure and Dynamics

RENÉ D. GARREAUD

*Department of Geophysics, University of Chile, Santiago, Chile*

(Manuscript received 7 June 1999, in final form 13 October 1999)

### ABSTRACT

Synoptic-scale incursions of midlatitude air moving into subtropical South America (to the east of the Andes Cordillera) are observed to occur year-round with a periodicity of about 1–2 weeks. During wintertime, they have a profound impact upon the low-level temperature field, and extreme episodes produce freezing conditions from central Argentina to southern Brazil and Bolivia. Warm season episodes produce less dramatic variations of temperature, but they organize deep convection in the form of synoptic-scale bands of convective cloudiness along the leading edge of the cool air. On the basis of 17 yr of NCEP–NCAR reanalysis and outgoing longwave radiation fields, the mean, synoptic-scale structure, and evolution of these incursions is documented, using a simple compositing technique. The underlying physical mechanisms responsible for the occurrence of these incursions are also investigated by diagnosing the leading dynamic and thermodynamic forcing of their development.

### 1. Introduction

Synoptic-scale incursions of cold, midlatitude air that penetrate into the subtropics are frequently observed to the east of major north–south-oriented mountain ranges (e.g., Riehl 1954; Ramage 1971; Hastenrath 1991; Slingo 1998). These so-called cold surges have a marked impact on regional weather (although their influence on tropical convection may lead to interactions on planetary scales) and, not surprisingly, literature focusing on episodes over specific regions is extensive. Particular emphasis has been placed on cold surges over southeastern Asia bounded by the Himalayan Plateau and their influence on the Tropics during the winter monsoon (e.g., Boyle and Chen 1987; Lau and Chang 1987; Wu and Chan 1995, 1997). Wintertime, intense cold surges along the east side of the Rockies have also attracted considerable interest due to their impact over the western side of the Great Plains of North America (e.g., Colle and Mass 1995) and their subsequent impact on Central America and the Caribbean (see Schultz et al. 1997 for an extensive review of the literature on Central American cold surges).

In South America, episodic incursions of midlatitude air to the east of the subtropical Andes (hereafter referred to as South American cold surges) occur year-round at intervals of 1–2 weeks. Extreme wintertime

episodes produce freezing conditions from central Argentina to southern Brazil, the chief agricultural sector of South America, which has motivated observational and numerical case studies (e.g., Hamilton and Tarifa 1978; Fortune and Kousky 1983; Marengo et al. 1997; Bosart et al. 1998; Garreaud 1999; see also Marengo et al. 1997 for further references). Summertime episodes produce less dramatic fluctuations in temperature and pressure, but they have been associated with bands of enhanced convection and rainfall (e.g., Ratisbona 1976; Parmenter 1976; Kousky 1979; Garreaud and Wallace 1998; Liebmann et al. 1999). From a statistical perspective, there is evidence that cold surges are the dominant synoptic-scale mode of circulation and temperature variability over subtropical South America. The leading modes in the extended EOF analysis performed by Kousky and Cavalcanti (1997) and Vera and Vignarolo (2000) capture the essential features of South American cold surges, and the classification of sea level pressure (SLP) patterns over southern South America presented by Compagnucci and Salles (1997) reveals that the “cold-surge mode” is the second more recurrent synoptic pattern after the zonal circulation. As shown in the appendix, cold surges have also a noticeable imprint upon the climatological distribution of low-level temperature and circulation over South America.

Most of the literature on South American cold surges has focused on descriptive aspects of individual episodes, especially those with large impact on southeastern Brazil. In this paper we document the mean, large-scale structure and evolution of cold air incursions bounded by the subtropical Andes. Our goal is threefold.

---

*Corresponding author address:* Dr. René D. Garreaud, Department of Geophysics, University of Chile, Blanco Encalada 2085, Santiago, Chile.  
E-mail: rgarreau@dgf.uchile.cl

First, we aim to produce a comprehensive “climatology” of this phenomenon that may be useful to place in context individual cases and infer their departures from the mean behavior. Second, the synoptic-scale dynamics of cold surges is investigated using the mean fields. Here we are mainly interested in the mechanisms that are responsible for the equatorward advance of the cold air, and the role of the large-scale forcing and the topography in the development of the incursions. Finally, we describe the seasonal dependence of cold surges (wintertime versus summertime episodes) in terms of their structural evolution and effects upon regional weather.

The paper is organized as follows. The data and methodology are presented in section 2. A description of the mean structure and dynamics of wintertime cold surges is presented in section 3. In section 4 we describe summertime cold surges, highlighting their similarities and differences with wintertime episodes. Finally, a conceptual model and a summary of our main findings are presented in section 5.

## 2. Data and methodology

The analyses in this work are based on 17 years (1979–95) of atmospheric reanalysis fields produced by the National Centers for Environmental Prediction–National Center for Atmospheric Research [the NCEP–NCAR reanalysis; see details in Kalnay et al. (1996)] and outgoing longwave radiation (OLR) field measured by polar-orbiting satellites (Liebmann and Smith 1996). Original NCEP–NCAR reanalysis data have a 6-h resolution and OLR fields are measured twice daily, but most of our analysis is based on daily averages. Both datasets are on  $2.5^\circ \times 2.5^\circ$  latitude–longitude grid, and the reanalysis includes all mandatory levels between 1000 and 10 hPa (300 hPa for humidity).

An important caveat in the use of the NCEP–NCAR reanalysis for studies over the Southern Hemisphere involves incorrectly assimilated (shifted by  $180^\circ$  of longitude) Australian surface pressure bogus data (PAOBs) between 1979 and 1992. Although this error must be kept in mind in interpreting the results presented here, we are still confident that the NCEP–NCAR reanalysis captures most of the features of our synoptic climatology. First, the most important features of South American cold surges are observed over a continental area to the north of  $40^\circ\text{S}$ , where there are few, if any, displaced PAOBs observations, and the assimilation of conventional data should strongly damp any errors that may propagate in from the southern Pacific. Second, our statistical analyses are based on a large number of episodes, which also should tend to reduce the impact of large differences during individual days.

To document the mean three-dimensional structure and evolution of cold surges over South America we

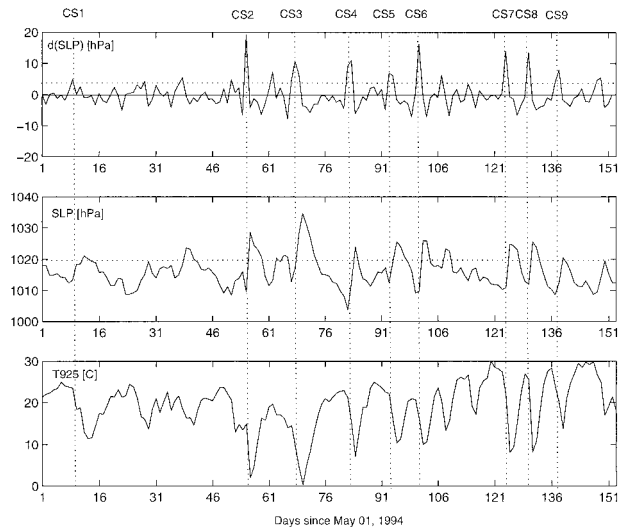


FIG. 1. Daily mean values of 24-h sea level pressure tendency ( $\delta\text{SLP}$ , upper panel), sea level pressure (middle panel), and 925-hPa air temperature (lower panel) averaged over a  $5^\circ \times 5^\circ$  grid box centered at  $25^\circ\text{S}$ ,  $57.5^\circ\text{W}$ , during the winter (May–Sep) of 1994. Horizontal, dashed line in the upper panel indicates the limit of the 10% frequency distribution of  $\delta\text{SLP}$  during this season. Vertical dashed lines indicate day 0 of the selected cold surges (CS1, CS2, . . . , CS9). Three of the events selected with this procedure produced damage in coffee growing areas in southeastern Brazil (CS2, 26 Jun; CS3, 9 Jul; and CS6, 10 Aug) according to Marengo et al. (1997).

have used a compositing analysis described next.<sup>1</sup> Since the steep rise in surface pressure at the leading edge of the surge is one of the best-defined features of both cold and warm season episodes, we have chosen the 24-h SLP tendency ( $\delta\text{SLP}$ ) as the key variable for case selection. The initial set of episodes was taken as the days that fall within the top 10% of the seasonal frequency distribution of  $\delta\text{SLP}$  in a  $5^\circ \times 5^\circ$  grid box centered at  $25^\circ\text{S}$ ,  $57.5^\circ\text{W}$ . To ensure that the marked SLP rise was actually associated with the passage of a strong anticyclone (and therefore with a cold surge) we only retained those episodes in which  $\text{SLP} \geq 1020$  hPa (1015 hPa for summer) following the pressure rise. As an example of this selection procedure, Fig. 1 shows the time series of  $\delta\text{SLP}$ , SLP, and 925-hPa temperature for the winter of 1994, together with the selected episodes. Three of the selected episodes during this winter produced severe damage in the coffee growing areas in southeastern Brazil, according to a list in Marengo et al. (1997).

<sup>1</sup> Recently, Vera and Vighiarolo (2000) also used a compositing analysis to describe cold air outbreaks over South America during wintertime. Their analysis is based on 6 yr of European Centre for Medium-Range Weather Forecasts analysis (1983–88). They applied a rotated extended empirical function (REEOF) analysis to the 850-hPa geopotential height fields and found that the fourth mode corresponds to cold air outbreaks over the continent. Then, a compositing analysis refers to the average over time when the REEOF-4 temporal coefficient is larger than 0.8 times the standard deviation of the series.

Application of this procedure to the  $\delta$ SLP time series from 1979 to 1995 yields a total pool of 145 wintertime episodes (May–September) and 132 summertime episodes (November–March) (about eight episodes per season). The day-0 composite field was defined as the average of the individual spatial fields during those “key” episodes. Composite fields for day  $n$  (for  $n = -2, -1, +1, \text{ and } +2$ ) are defined as the average of the fields during  $n$  days before or after each original day 0. The associated circulation, convective activity, and thermodynamic features are characterized by extending the compositing analysis to several other meteorological fields.

Composite anomalies were determined as the difference between the composite maps and the 17-yr seasonal means, and tested for statistical significance using a two-tailed Student’s  $t$ -test. More important, spatial and temporal coherence and dynamical consistency of the features of our composites constitute the most convincing proof that we have incorporated enough events into the composite to ensure that the “signal” stands out well above the sampling variability.

### 3. Wintertime cold surges

#### *a. Large-scale circulation at upper levels*

The large-scale circulation at middle and upper levels over South America during wintertime cold surges is characterized by a midlatitude wave, with a ridge to the west of the Pacific coast of the continent and a trough extending southeastward from the subtropics into the South Atlantic (Fig. 2). Such configuration produces strong advection of anticyclonic vorticity (AVA) aloft to the east of the Andes between  $40^\circ$  and  $30^\circ\text{S}$  (Fig. 3). The wave exhibits significant amplification before and during the mature stage of the cold surge (day 0 in our composite) as it drifts eastward at about  $12 \text{ m s}^{-1}$ . Krishnamurti et al. (1999) have shown that the large amplitude of the ridge–trough couplet during these episodes arises from the superposition of fast-moving, synoptic-scale waves and quasi-stationary, planetary waves. Yet, the largest amplification of the upper-level wave during the mature stage of the cold surge is largely due to baroclinic growth of the synoptic wave as cold air at low levels moves northward beneath the axis of the upper-level trough (Marengo et al. 1997; Krishnamurti et al. 1999). The NW–SE orientation of the trough and ridge axes is also characteristic of extratropical, transient waves as they move to the lee of the Andes (e.g., Gan and Rao 1994; Berbery and Vera 1996; Seluchi et al. 1998).

Southwesterly flow, downstream from the ridge axis, turns eastward over the subtropical part of the continent, into a confluent region at the entrance of a jet stream in the equatorward flank of the trough (Fig. 2b). The existence of such a jet entrance region appears as an important large-scale feature during strong, long-lasting

cold incursions, as seen in the individual members of our composite (not shown) and case studies reported in the literature. The acceleration of the horizontal wind induces a direct, secondary circulation cell in the plane normal to the jet axis (e.g., Uccellini and Johnson 1979), with downward (upward) motion on the poleward (equatorward) side of the jet. Thus, midtropospheric subsidence over south-central Argentina acts in concert with AVA aloft, while rising motions at lower latitudes induce midlevel adiabatic cooling and favor the incursion of the cold air. The existence of upper-level, subtropical jet entrance regions is also an important ingredient in the occurrence of strong, long-lived cold surges over northern Central America (Schultz et al. 1998) and southeast Asia (Lau and Chang 1987).

#### *b. Low-level pressure and wind fields*

Figure 4 shows the composite sequence of 1000-hPa geopotential height and low-level winds for wintertime episodes. By the onset of the system (day  $-1$ ) a migratory high pressure center has strengthened the South Pacific anticyclone off the coast of southern Chile and begins to move into southern Argentina around  $40^\circ\text{S}$  (Fig. 4a), where the height of the Andes Cordillera does not exceed 2000 m. At the same time, an elongated trough extends from the central part of the continent into the southern Atlantic Ocean, where it merges with a low pressure center. Within the next 24 h (day 0) the area of high pressure evolves into a tight, intense anticyclone ( $1020+$  hPa) centered to the east of the Andes at  $33^\circ\text{S}$ , while the low-level trough deepens off the eastern coast of South America (Fig. 4b). Marengo et al. (1997) and Garreaud (1999) have shown evidence that strong quasigeostrophic vorticity advection within the upper-level wave is the leading contributor to the growth of both the continental anticyclone (to the south of  $30^\circ\text{S}$ ) and the marine cyclone. Finally, on days  $+1$  and  $+2$  the core of the continental high pressure weakens, as it slowly drifts eastward (Fig. 4c). However, ridging still takes place along the eastern slope of the Andes, fostering the advance of the northward flank of the surface anticyclone as far north as  $10^\circ\text{S}$ .

Under quasigeostrophic conditions, the pronounced low-level meridional pressure gradient over the subtropical plains of the continent implies a predominantly easterly flow. In contrast, the composite low-level flow is dominated by a southerly, terrain-parallel component, and the wind is largely downgradient near the leading edge of the cold air (Figs. 4b, 5b). Southerly flow to the east of the Andes extends all the way from surface to the upper troposphere, but the strongest winds ( $v \geq 12 \text{ m s}^{-1}$ ) are found below the 700-hPa level (Fig. 7). We speculate that the departure from geostrophy arises mainly from the blocking effect of the subtropical Andes (with a representative height  $h_m \sim 3000 \text{ m}$ ), since for the observed range of upstream flow ( $U \sim 10 \text{ m s}^{-1}$ ) and static stability ( $N \sim 1.8 \times 10^{-2} \text{ s}^{-1}$ ), the ratio of

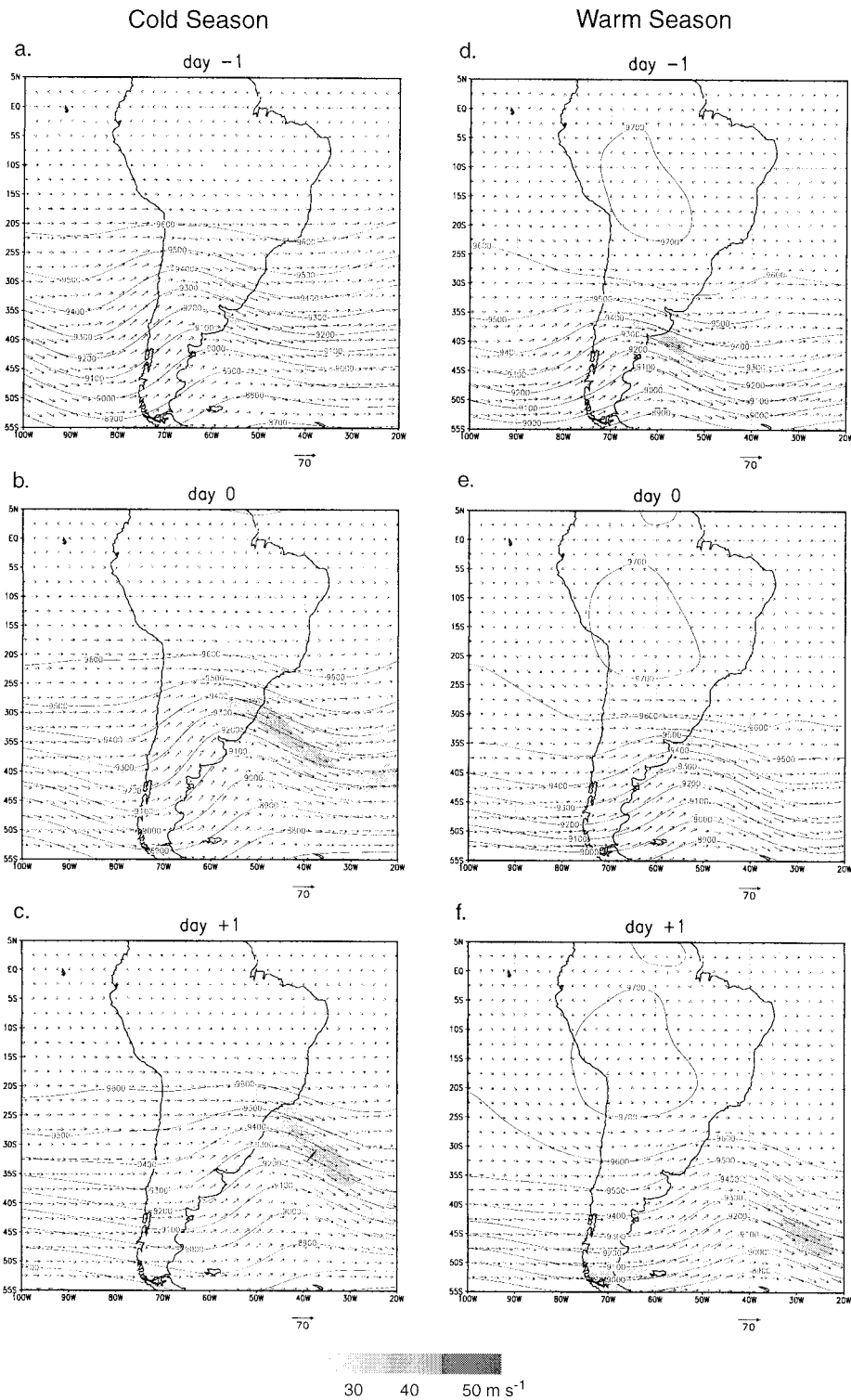


FIG. 2. Composite maps of 300-hPa wind vectors, geopotential height (contoured every 100 m), and isotachs (shaded) for cold surges during winter (left panels) and summer (right panels). Reference vectors are at the bottom of the figures.

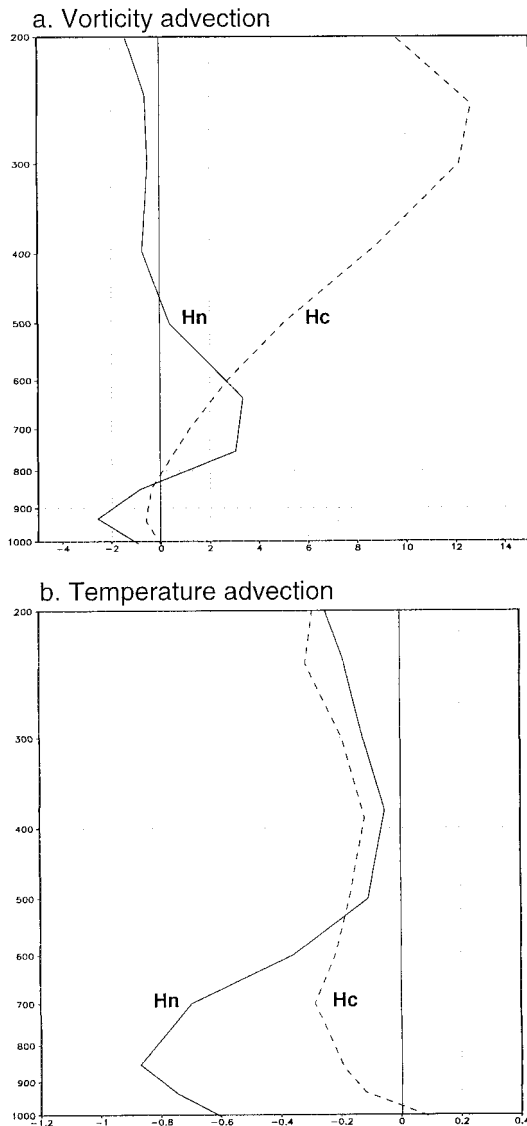


FIG. 3. (a) Wintertime composite vertical profiles of relative vorticity tendency (units:  $10^{-5} \text{ s}^{-1}$ ) averaged over the boxes Hc (solid line) and Hn (dashed line) on day 0. Both boxes are  $2^\circ \times 2^\circ$ . Here, Hc is centered at  $33^\circ\text{S}$ ,  $60^\circ\text{W}$  (nearly the core of the anticyclone on day 0); Hn is centered at  $18.5^\circ\text{S}$ ,  $60^\circ\text{W}$  (near the leading edge of the cold air on day 0). (b) As in (a) but for the horizontal advection of temperature (units:  $10^{-4} \text{ K s}^{-1}$ ).

kinetic energy of the approaching flow to potential energy needed to pass over the mountain range, measured by the Froude number  $\text{Fr} = U/h_m N$ , is much less than unity ( $\text{Fr} \sim 0.20$ ). The band over which the composite low-level flow departs from geostrophy is about 900 km wide (away from the Andes), consistent with the theoretical scale for upstream deceleration under persistent blocking [i.e., the Rossby radius of deformation,  $l_R$ ; e.g., Pierrehumbert and Wyman (1985)]. Table 1 shows values of  $\text{Fr}$  and  $l_R$ , for both wintertime and summertime composite cold surges.

The blocking of the flow normal to the barrier leads

to the damming of cold air against the eastern side of the Andes. The theoretical study by Xu (1985) indicates that, for steady-state conditions, the mountain-parallel (meridional) jet is maintained by a balance between the synoptic-scale, mountain-parallel pressure gradient and friction. In the cross-barrier (zonal) direction, the pressure gradient force induced by the cold dome (directed away from the barrier) is balanced by the Coriolis force acting upon the along-barrier wind, and together they control the shape of the cold dome. At the leading edge of the cold air, however, the surface friction does not balance the strong meridional pressure gradient, resulting in a northward acceleration of the surface winds. Finally, as cold air advances northward of  $18^\circ\text{S}$ , the blocking effect subsides but the flow is still largely downgradient because the Coriolis force becomes too small. Results from the numerical simulation in Garreaud (1999) suggest that this conceptual model captures the essence of the momentum balance within the cold air region.

### c. Low-level temperature field

Concomitant with the equatorward expansion of the surface anticyclone and the ageostrophic southerly flow, a tongue of cold air moves into low latitudes to the east of the Andes (Figs. 5, 6). As shown in the latitude–pressure sections in Fig. 7, temperature (and humidity) anomalies are found through most of the troposphere, connected with the midlatitude trough, but the largest cooling takes place below 700 hPa, over an elongated sector extending southeastward from the eastern slope of the Andes. At  $25^\circ\text{S}$ , the mean near-surface cooling rate during wintertime cold surges is about  $5^\circ\text{C day}^{-1}$ , but in individual episodes, the maximum cooling (derived from reanalysis data) can be as large as  $10^\circ\text{C (12 h)}^{-1}$ . According to mesoscale simulations by Garreaud (1999) and Knight and Bosart (1988), the leading edge of the cold air is characterized by a frontlike baroclinic zone [ $\sim 4^\circ\text{C (100 km)}^{-1}$ ] with nearly vertical isentropes below the 800-hPa level and a sharp shift of the meridional low-level wind.

The differential temperature advection produced by the advance of a shallow dome of cold air is in turn responsible for the ridging along the Andes northward of  $20^\circ\text{S}$  (note that at these low latitudes vorticity advection in the tropospheric column is small; Fig. 3). The contribution of the shallow incursion of cold air in raising the surface pressure can be estimated by integrating the hydrostatic equation across the cold air dome:

$$\Delta p_H = -gp_0/(RT^2)H\Delta T, \quad (1)$$

where  $\Delta p_H$  is the hydrostatic pressure change,  $T$  is the mean temperature of the cold dome,  $H$  is depth of the cold air, and  $\Delta T$  is the temperature perturbation induced by the cold dome. In addition,  $p_0$  is a surface pressure reference,  $g$  is gravity, and  $R$  is the ideal gas constant. From our wintertime composite, we obtain  $T \sim 280 \text{ K}$ ,

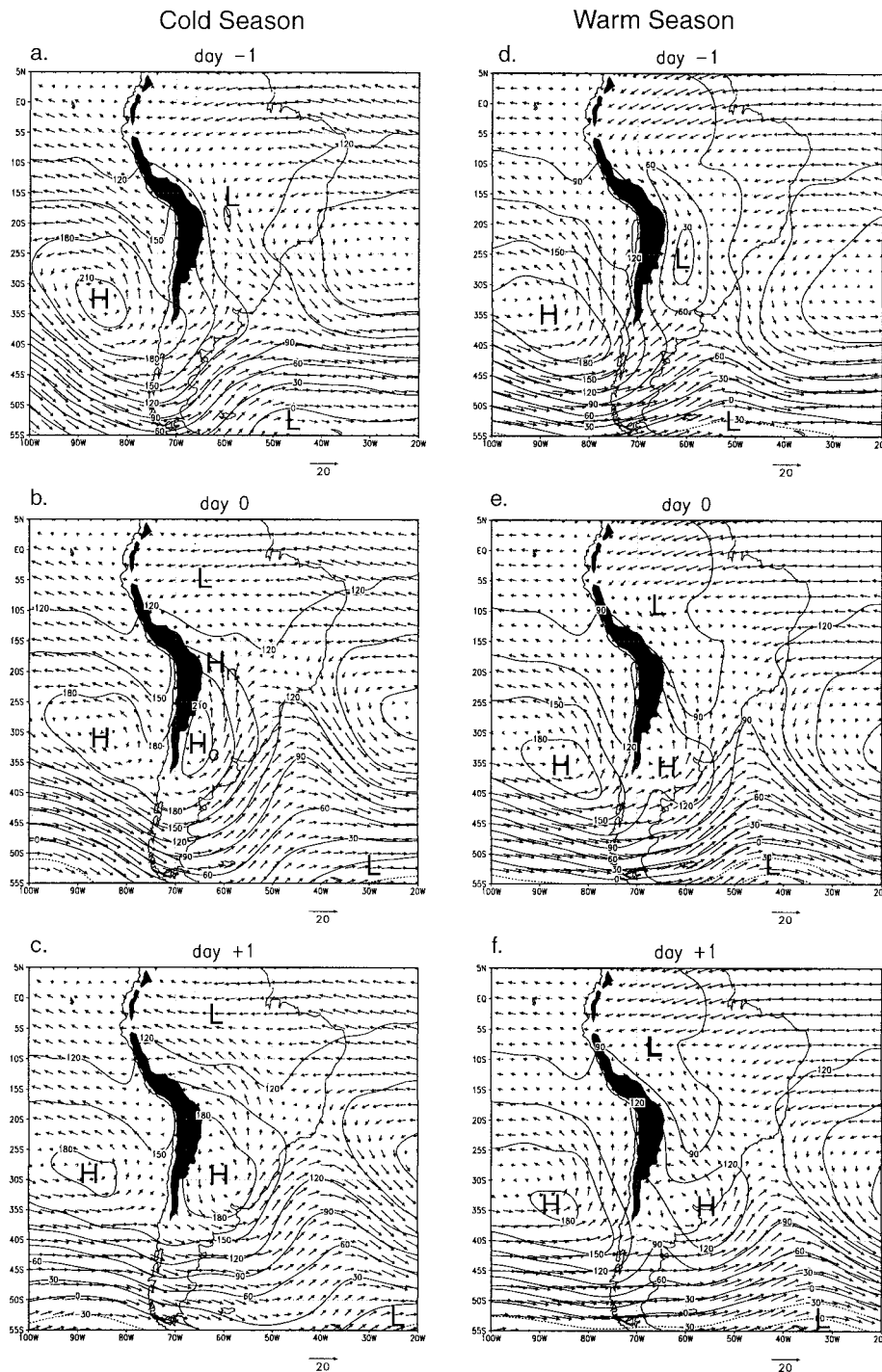


FIG. 4. Composite maps of low-level (1000–850 hPa) wind vectors and 1000-hPa geopotential height (contoured every 30 m) for cold surges during winter (left panels) and summer (right panels). Black areas indicate terrain elevation in excess of 1000 m. Low and high pressure centers indicated by L and H, respectively. Reference vectors are at the bottom of the figures.

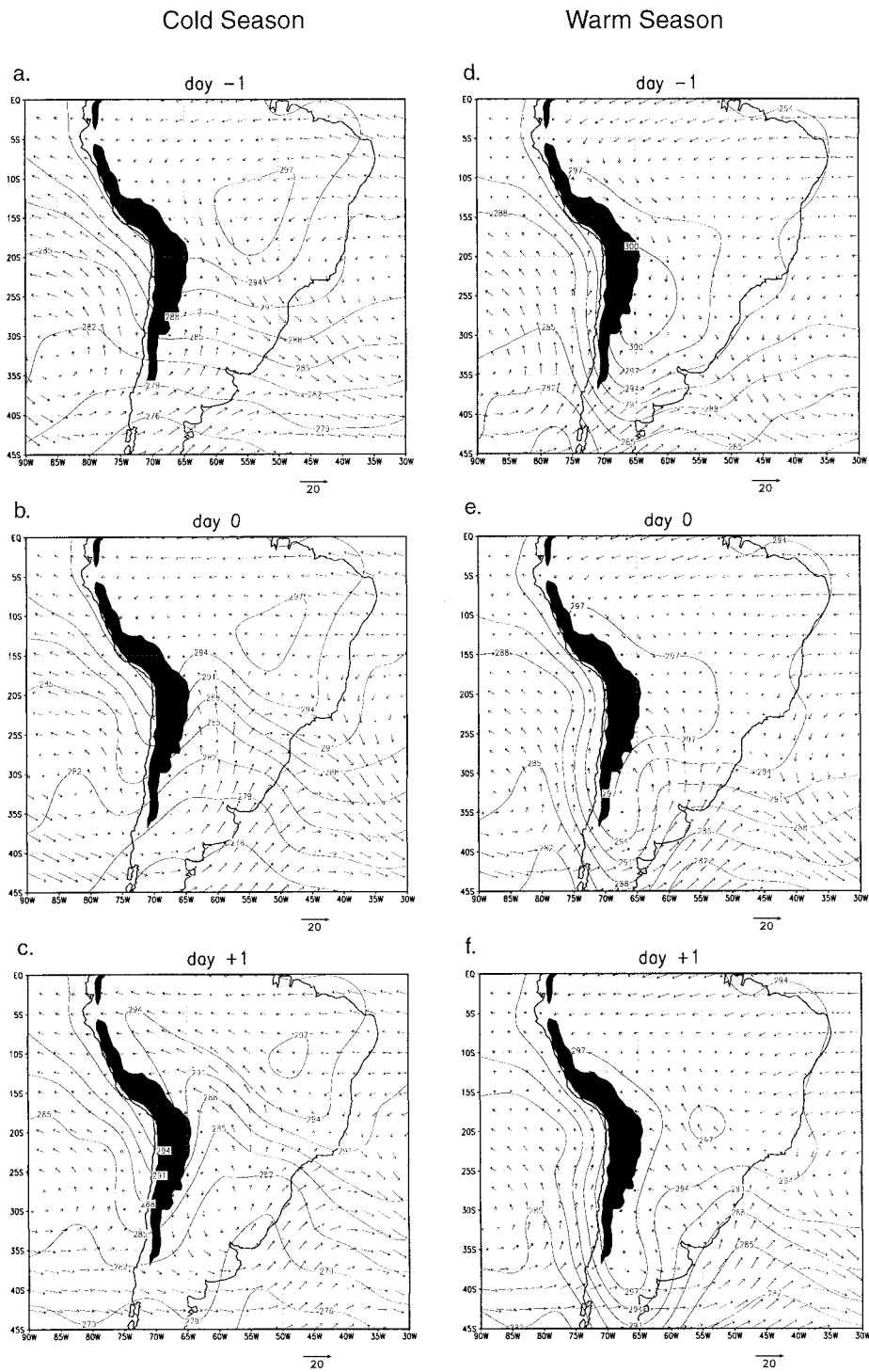


FIG. 5. Composite maps of low-level (1000–850 hPa) wind vectors and 925-hPa air temperature (contoured every 3 K) for cold surges during winter (left panels) and summer (right panels). Black areas indicate terrain elevation in excess of 1000 m. Reference vectors are at the bottom of the figures.

TABLE 1. Scaling analysis of the composite low-level flow to the east of the subtropical Andes during cold surges at days 0 and +1. The following parameters characterize the eastern slope of the subtropical Andes:  $l_m \sim 300$  km (half-width) and  $h_m \sim 3000$  km (height).  $f$  = Coriolis parameter.  $V$  = magnitude of the meridional low-level wind estimated from Figs. 1 and 2.  $N$  = Brunt-Väisälä frequency, averaged between 1000 and 700 hPa.  $Ro$  = Rossby number;  $Ro = U/fh_m$ , where  $U = 12$  m s<sup>-1</sup> in all cases.  $L_R$  = Rossby radius of deformation;  $L_R = Nh_m/f$ .  $L_O$  = observed width of the meridional flow anomalies (estimated from Figs. 1–3).

Parameter	30°S ( $f = -7.3 \cdot 10^5$ s <sup>-1</sup> )		20°S ( $f = -4.9 \cdot 10^5$ s <sup>-1</sup> )	
	Day 0		Day +1	
	Wintertime	Summertime	Wintertime	Summertime
$V$ (m s <sup>-1</sup> )	15	15	10	8
$N$ 10 <sup>-2</sup> (s <sup>-1</sup> )	1.9	1.6	1.6	1.3
$Ro$	0.68	0.55	0.65	0.53
$L_R$	900	750	1100	900
$L_O$ (km)	1000	900	1000	900

$H \sim 2000$  m, and  $p_0 \sim 1010$  hPa. Then, near 20°S the low-level temperature change between days 0 and +1,  $\Delta T \sim -6$  K, implies a pressure change of  $\Delta p_H \sim +5$  hPa, very similar to the observed total pressure change.

To determine the origin of the low-level cooling we evaluated the thermodynamic energy equation at the 925-hPa level:

$$\partial T/\partial t = -\mathbf{V} \cdot \nabla T + \omega S_p + \mathfrak{H}, \quad (2)$$

where  $\mathbf{V} = (u, v)$  is the horizontal wind,  $\omega$  is the vertical velocity,  $S_p$  is the static stability parameter, and  $\mathfrak{H}$  represents the aggregated effect of the diabatic heating and vertical advection. Figure 8 shows the local rate of cooling ( $\partial T/\partial t$ ), the horizontal temperature advection ( $-\mathbf{V} \cdot \nabla T$ ), and the adiabatic cooling ( $\omega S_p$ ) at day 0 using the composite fields for wintertime and summertime cold surges. Within the region of the cold air, horizontal advection largely dominates the local cooling in both cold and warm season episodes: the large-scale structure and amplitude of the total ( $\partial T/\partial t$ ) and advective ( $-\mathbf{V} \cdot \nabla T$ ) cooling rates agree closely. The horizontal advection of temperature is in turn dominated by its meridional component ( $-v\partial T/\partial y$ ), consistent with the similarity between the phase speed of the leading edge of the system and the low-level wind speed behind it ( $\sim 10$  m s<sup>-1</sup>). Marengo et al. (1997) and Vera and Vignarolo (2000) also evaluated the thermodynamic energy equation at different levels for cold surges with greatest impact over southeast Brazil using reanalysis data. In agreement with our results, they found that low-level cooling is largely produced by horizontal cold advection, but also noticed that large-scale rising motion has a larger contribution in the cooling of the middle troposphere over subtropical South America. The absence of significant rainfall over the continent during wintertime “dry” episodes suggests that moist processes are not essential for the equatorward advance of the cold air. During summertime episodes, however, evaporative

cooling underneath areas of deep convection might be a more significant factor in the thermodynamic balance.

#### 4. Summertime episodes and interaction with convection

The composite fields for summertime episodes are presented side by side with their wintertime counterparts in Figs. 2, 4, and 5. Summertime and wintertime composite episodes exhibit a similar structure and evolution, and the weaker and more diffuse features in the *full* fields of the warm season incursions arises, at least partially, from seasonal differences in the mean circulation and thermodynamic conditions: the presence of a deep thermal trough over the central part of the continent and the weakening and southward displacement of the large-scale temperature gradient over the southern tip of South America. The former masks the northward advance of the cold anticyclone, while the later results in weaker upper-level transient waves.

The *anomalies* of the meridional wind and  $\theta_e$  (Fig. 6) clearly reveal the equatorward advance of the southerly winds and cold air, with amplitude and scale comparable to the wintertime composite. The surface pressure anomalies (not shown) and the vertical structure of summertime and wintertime episodes (Fig. 7) are also similar. Nevertheless, important seasonal differences are (a) the northerly, presurge flow is stronger during the onset of the warm season episodes, intensifying the advection of warm, humid air over the central part of the continent (Fig. 6d), and (b) negative  $\theta_e$  anomalies remain stationary to the south of 20°S during the later stage of warm season episodes (Figs. 6f, 7f), presumably as a result of strong heat fluxes over the central part of the continent, leading to an increasing separation between the low-level southerly winds and the cold air.

An aspect better defined and relevant in summertime “cool surges” is their impact upon deep convection. Figure 9 shows the composite sequences of the convective index (CI) and its departures from the seasonal mean (CI anomalies). The CI is defined as 230-OLR if  $OLR < 230$  W m<sup>-2</sup> or 0 otherwise, so that it increases with colder cloudiness. No signature of CI is evident over the continent during the wintertime composite. During summertime, a band of positive CI anomalies (enhanced convection) at the leading edge of the cool air moves from the southern subtropics ( $\sim 35^\circ$ S) into lower latitudes (as north as 5°S) in about 4 days. This synoptic-scale band is limited by the eastern slope of the Andes and extends into the South Atlantic with a NW–SE orientation. The enhanced convection ahead of the summertime cool surges is consistent with the intense low-level wind convergence embedded in a conditionally unstable environment.

The occurrence of elongated bands of deep convection ahead of cold air incursions over subtropical South America has been documented on case studies by Ra-

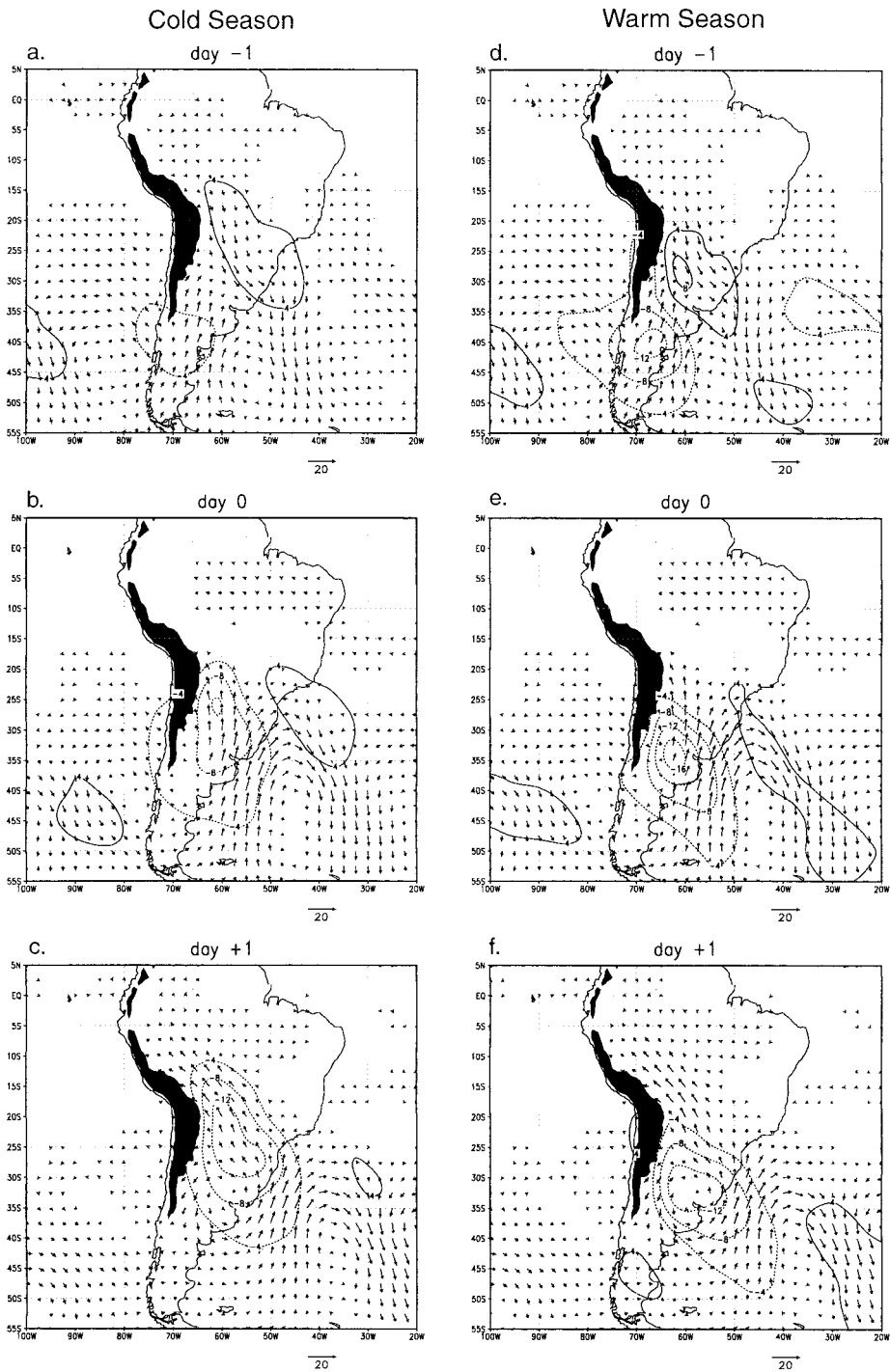


FIG. 6. Composite maps of low-level (1000–850 hPa) wind anomaly and 925-hPa equivalent potential temperature anomaly ( $\theta_e$ , contoured every 4 K) for cold surges during winter (left panels) and summer (right panels). Anomalies are calculated as departures from seasonal mean. Only wind anomalies locally statistically significant at the 95% confidence level are shown. Reference vectors are at the bottom of the figures. The  $\theta_e$  anomalies in excess of  $\pm 2.5$  K are statistically significant at the 95% confidence level over most of the domain. Black areas indicate terrain elevation in excess of 1000 m.

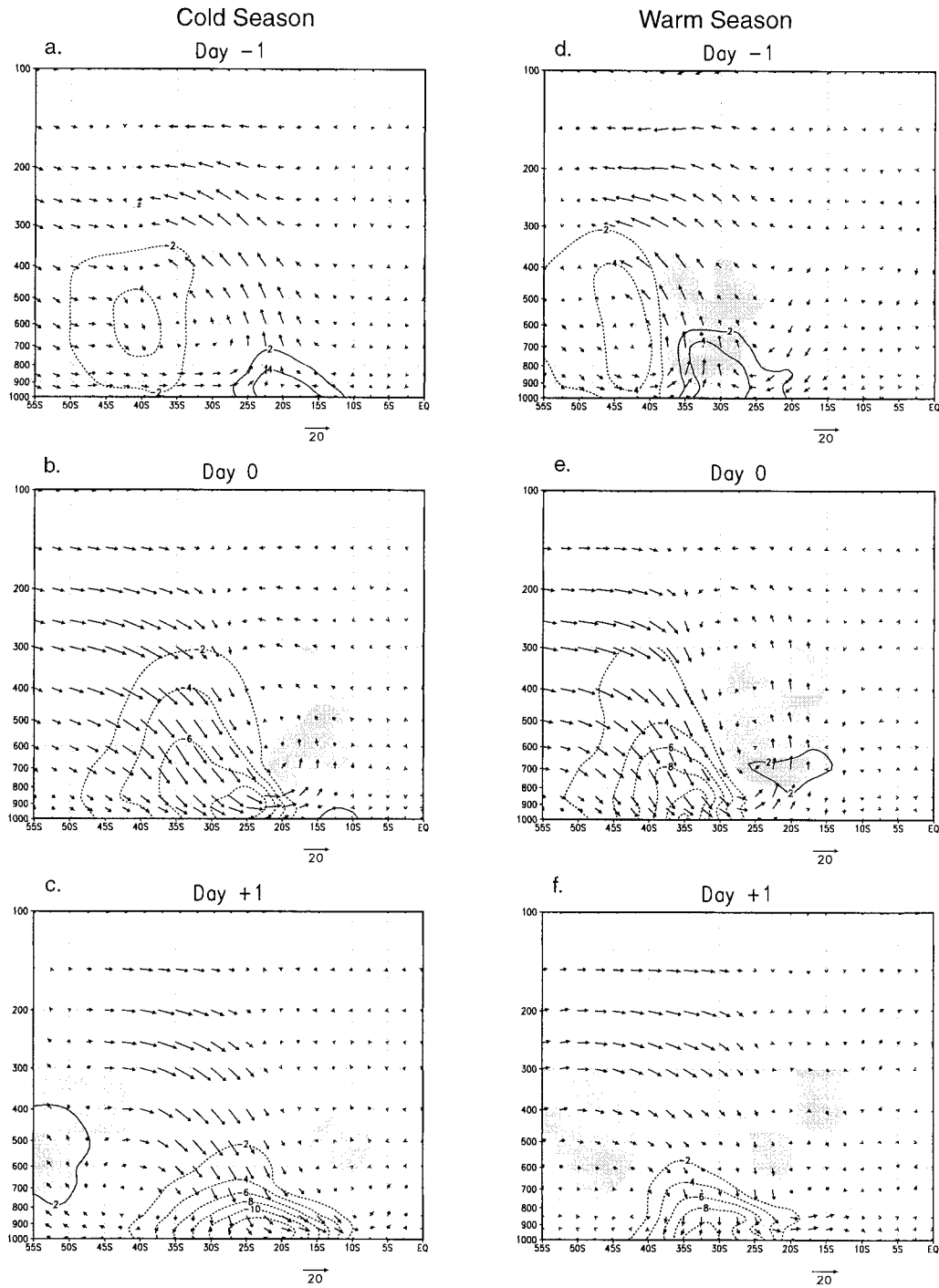


FIG. 7. Composite anomalies of the meridional circulation ( $v, w$ ), potential temperature ( $\theta$ , contours), and specific humidity (shaded) along  $60^\circ\text{W}$  for cold surges during winter (left panels) and summer (right panels). Anomalies are calculated as departures from seasonal mean. The contour interval for  $\theta$  is 2 K, dashed lines indicate negative values, and the zero contour is omitted. Reference vectors are at the bottom of the figures ( $20 \text{ m s}^{-1}$  horizontal,  $20 \text{ mm s}^{-1}$  vertical). Shading indicates specific humidity anomaly in excess of  $1 \text{ g kg}^{-1}$ .

tisbona (1976), Parmenter (1976), Fortune and Kousky (1983), and Garreaud (1999). It is also evident in the regression analyses between OLR and circulation over South America presented in Kiladis and Weickmann

(1997) and Liebmann et al. (1999). Kousky (1979) and Kousky and Ferreira (1981) established the influence of “cold fronts or their remains” on convective rainfall along the northeast coast of Brazil and the Amazon

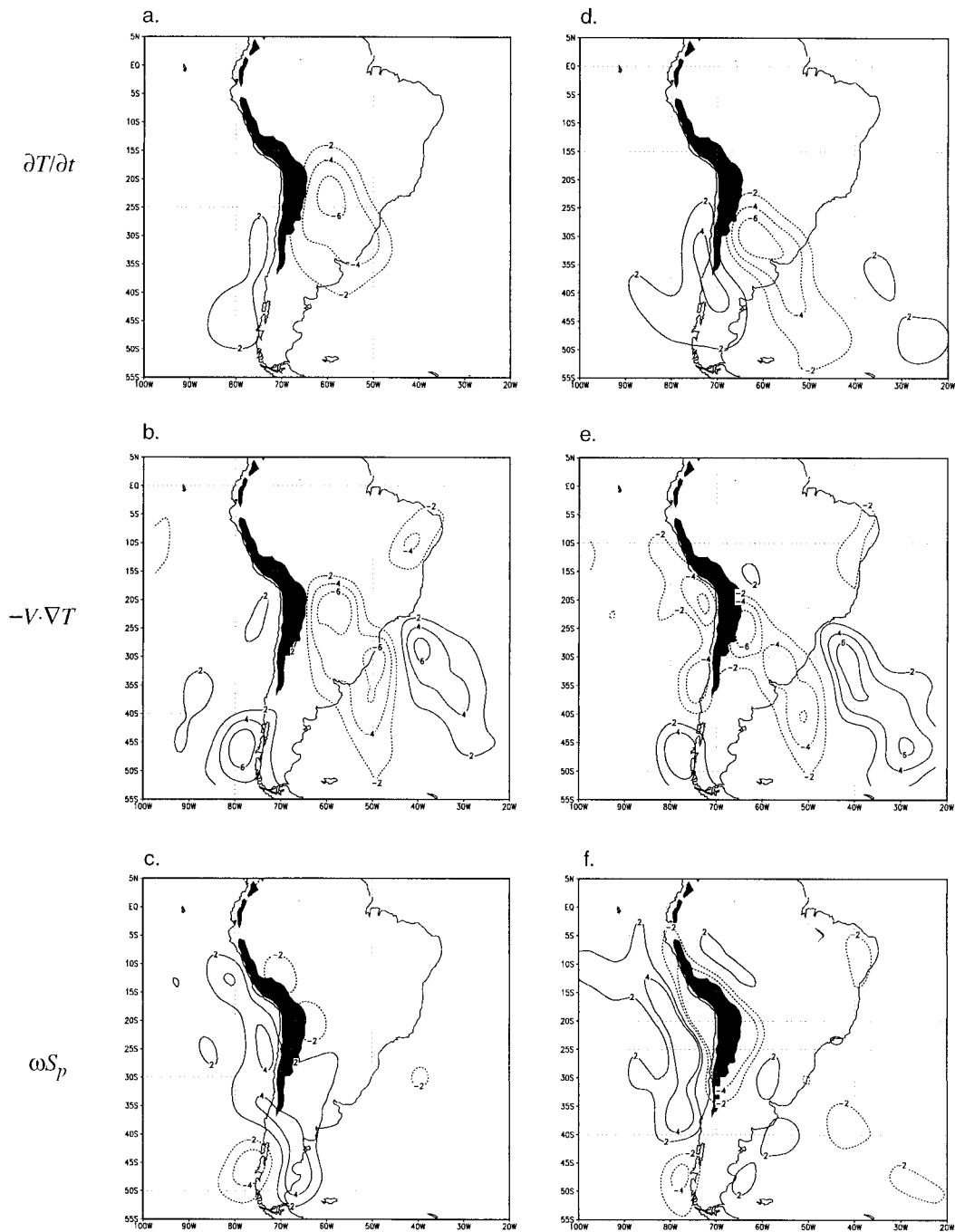


FIG. 8. Leading terms in the thermodynamic energy equation on day 0 for cold surges during winter (left panels) and summer (right panels) evaluated at the 925-hPa level. In all panels the contour interval is  $2 \text{ K day}^{-1}$ , negative values are in dashed lines, and the zero contour is omitted. The terms are the local time rate of change of temperature (upper panels), the horizontal temperature advection (middle panels), and the adiabatic cooling (lower panels). Black areas indicate terrain elevation in excess of 1000 m.

Basin, particularly in December and January, and Montes de Oca (1995) described the association between cold air outbreaks and precipitation episodes along the eastern slope of the central (Bolivian) Andes. Garreaud and Wallace (1998) estimated the effect of these bands on the regional precipitation by compositing the pre-

cipitation rate field (from NCEP–NCAR and National Aeronautics and Space Administration/Data Assimilation Office reanalyses) and concluded that they account for about 50% of the total summertime precipitation south of  $25^{\circ}\text{S}$  and  $\sim 30\%$  over the west side of the Amazon Basin.

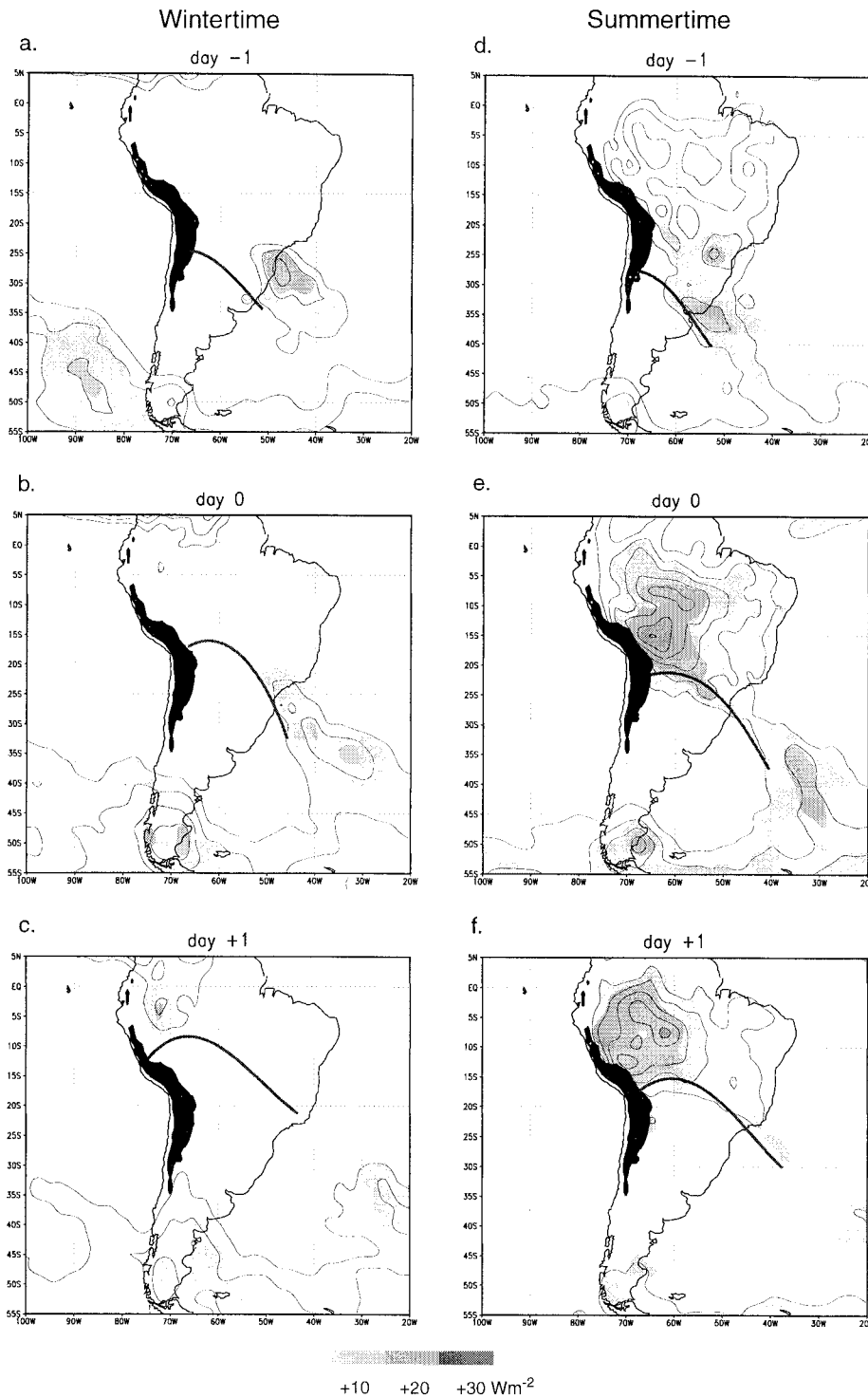


FIG. 9. Composite maps of CI (contoured every  $10 \text{ W m}^{-2}$ , beginning at  $+10 \text{ W m}^{-2}$ ), and CI anomalies (shaded) for cold surges during winter (left panels) and summer (right panels). Anomalies are calculated as departures from seasonal mean. Black areas indicate terrain elevation in excess of 1000 m. Thick solid lines indicate the leading edge of the surge at each day.

## 5. Conclusions

Evidence presented in this study and previous works indicates that cold surges along the east side of the Andes is the leading mode of synoptic-scale variability of the low-level circulation over most of subtropical South America. Wintertime episodes have a pronounced impact in the low-level air temperature, occasionally causing freezing conditions over subtropical regions. Summertime cool surges organize convective activity and rainfall in the form of synoptic-scale bands of enhanced deep convection flanked by areas where convection tends to be suppressed.

Case studies indicate a recurrent, well-defined large-scale structure during wintertime incursions of cold air over subtropical South America, so that our compositing analysis captures the essential features of this phenomenon. Summertime episodes and their composite exhibit a weaker and more diffuse structure, but their evolution and associated anomalies are similar to those of their wintertime counterpart. In both cases, the large-scale circulation at midlevels is characterized by a midlatitude, long wave, with a ridge immediately to the west of the Andes and a downstream trough over eastern South America and the southwestern Atlantic. The wave exhibits downstream amplification before and during the mature stage of the cold air incursion.

The synoptic-scale evolution near the surface is schematically illustrated in Fig. 10, generally applicable for wintertime and summertime episodes. Key elements are the surface cold core anticyclone that moves from the southeastern Pacific into southern Argentina, and a low center deepening over the southwestern Atlantic. To the south of 30°S, both the continental anticyclone and marine cyclone grow mainly at the expense of upper-level vorticity advection within the midlatitude baroclinic wave, in a manner similar to the development of such synoptic features elsewhere. The existence of an upper-level jet entrance over subtropical South America is instrumental in the occurrence of strong, long-lived cold surges, because it induces transverse, direct circulation that provides additional forcing to the central part of the surface anticyclone, and midlevel cooling at lower latitudes. To the north of 20°S, the direct effect of the large-scale circulation upon the low-level circulation is small, and the increase of surface pressure at the leading edge of the anticyclone is mostly explained by the hydrostatic effect of the shallow ( $H \sim 2000$  m) cold air moving northward.

At the onset of the cold air incursion (Fig. 10a) *geostrophic* southerly wind (between the high and low pressure cells) produces low-level cooling along the east coast of South America and farther inland as far north as 25°S. Studies of cold outbreaks that have a major impact over the eastern side of the continent have emphasized the rapid development of the surface cyclone over the southwest Atlantic. In these cases, southerly flow along the western flank of the low produces strong

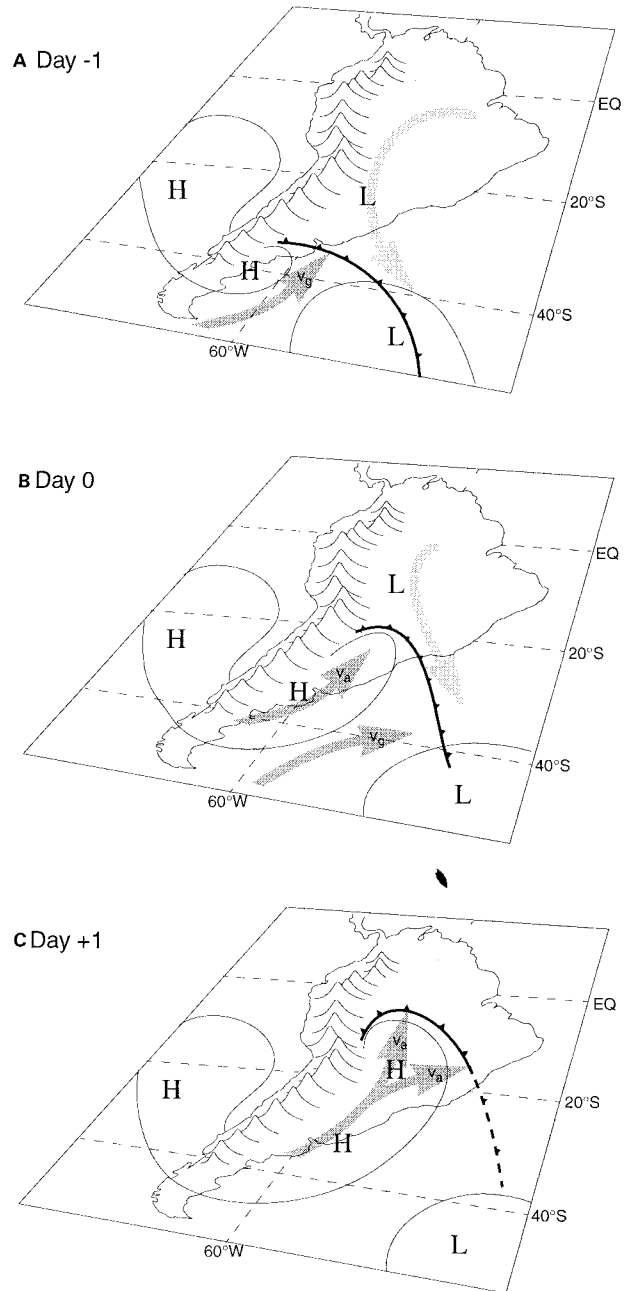


FIG. 10. Conceptual model of a cold air incursion over South America, generally applicable for wintertime and summertime episodes. Dark (light) thick arrows represent low-level wind advecting cold (warm) air. Thin contours represent surface isobars. Cold front at surface is shown conventionally. See text for details.

cold advection over central Argentina and southern Brazil (e.g., Marengo et al. 1997). Closer to the subtropical Andes, however, the low-level flow is totally blocked, leading to ageostrophic, terrain-parallel flow (Fig. 10b) and cold air damming. As the cold air moves into lower latitudes (Fig. 10c), the blocking effect of the Andes is diminished (due to a more zonal orientation of the Andes to the north of 18°S) but the ageostrophic balance still

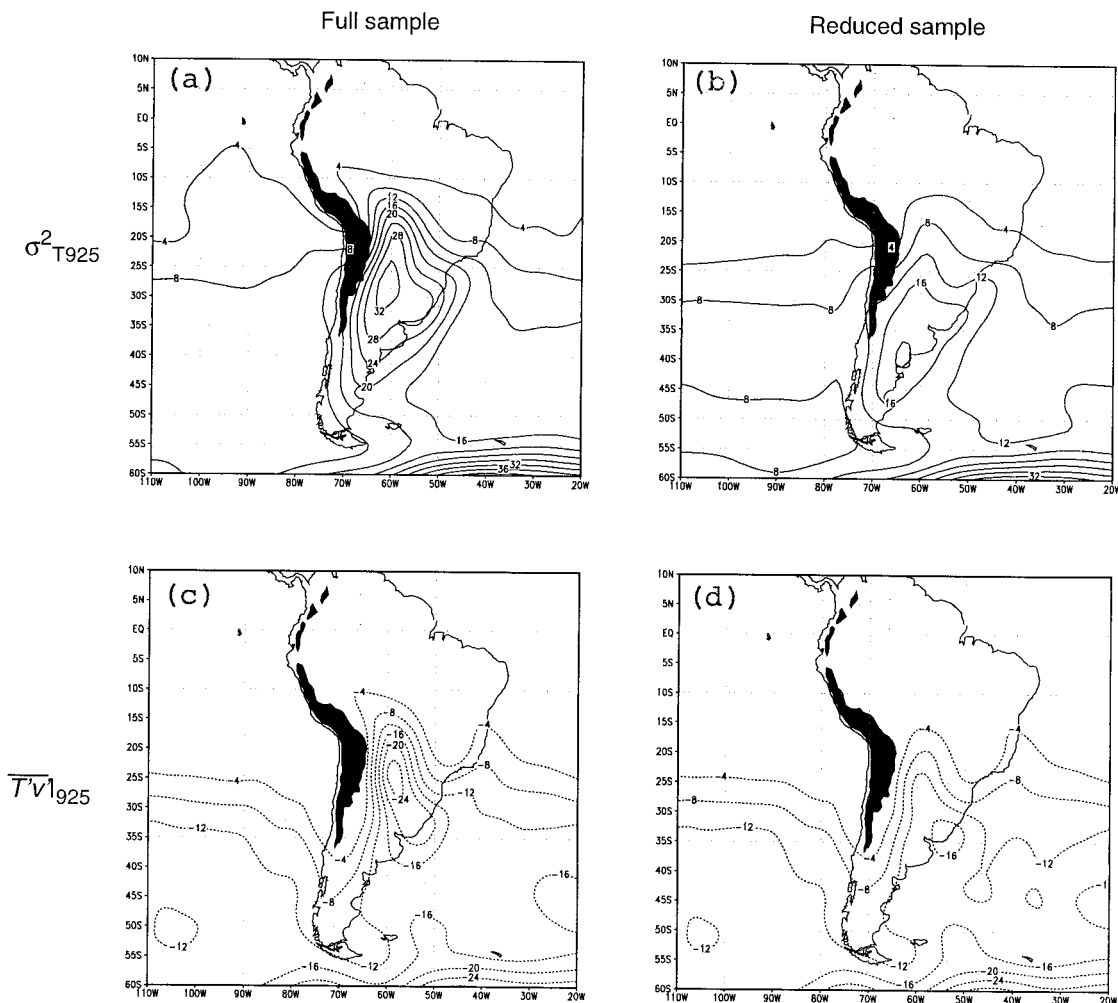


FIG. A1. Variance of air temperature at the 925-hPa level (upper panels) and mean 925-hPa meridional heat transport by transient eddies ( $\overline{T'v'}$ ) (lower panels) during the austral winter (May–Sep). The right panels are based on the full dataset (all winter days). The right panels are based on a reduced sample that does not include cold episodes (see text for details). Black areas indicate terrain elevation in excess of 1000 m.

prevails because the adjustment back to geostrophy is quite slow at these low latitudes. Cold advection produced by the southerly wind produces most of the local cooling at the leading edge of the surge. Since to the south of 35°S the cold air has moved into the South Atlantic and warm advection is set up, the dome of cold air at lower latitudes becomes cutoff from midlatitudes about 4 days after its onset.

In summary, the advance of the cold air incursion along the subtropical Andes is set up by the topographic blocking of the synoptic-scale flow. The subsequent spread over low latitudes, however, arises from a two-way interaction between the mass and wind fields: the strong pressure (temperature) gradient produces the acceleration of the low-level winds parallel to the Andes range (ageostrophic force balance in the along-mountain direction) while the horizontal advection of cold air by ageostrophic southerly flow maintains the strong tem-

perature gradient against dissipation by surface heat fluxes. Additionally, topographic Rossby waves and Kelvin waves do not appear to adequately explain the phenomenon documented in this paper, because of the dominance of horizontal advection in producing the low-level cooling.

While in this work we have emphasized the mean, large-scale aspects of cold air incursions over South America, there are many remaining questions regarding the relative importance of local (e.g., soil moisture) versus remote elements in producing case-to-case variability, predictability issues, and interannual variability of this phenomenon. We hope to address some of these topics in future work.

*Acknowledgments.* NCAR–NCEP reanalysis and OLR data were provided by the NOAA Climate Diagnostics Center. The author gratefully acknowledges

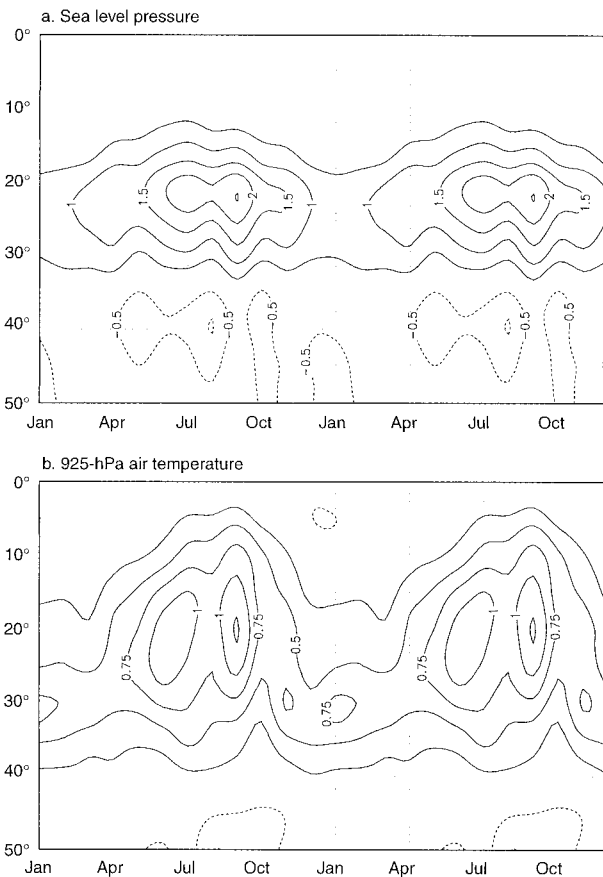


FIG. A2. (a) Annual march of the long-term mean standard deviation of sea level pressure along  $57.5^{\circ}\text{W}$ . The zonal mean at each latitude was removed and SLP was bandpass filtered to retain fluctuations in the 3–12-day range. (b) As for (a) but for 925-hPa air temperature.

the support and advice of Dr. John M. Wallace during the course of this work. Thanks are also due to Drs. J. Rutllant and H. Fuenzalida for comments and a careful reading of the manuscript. The comments of two anonymous reviewers led to substantial improvements in the presentation and content of this paper. This work represents a portion of the author's Ph.D. dissertation at the University of Washington and was supported by the National Science Foundation under Grant 9215512 and by the Departments of Geophysics and Research and Development of the University of Chile.

## APPENDIX

### Climatological Aspects

The wintertime (June–July–August) variance of the daily average of air temperature at 925 hPa ( $T_{925}$ ) over South America is shown in Fig. A1a. This field exhibits a maximum to the east of the subtropical Andes ( $\sim 25^{\circ}\text{S}$ ) extending as far north as  $10^{\circ}\text{S}$ , which indicates that the low-level temperature in this region experiences a de-

gree of high-frequency variability well above the background at low latitudes. To evaluate the influence of the cold surges upon this field, we recalculate the wintertime variance of  $T_{925}$  using a subsample of dates in which we exclude the most intense cold-surge episodes (see section 2). The variance map based on this reduced sample is shown in Fig. A1b. The variance of  $T_{925}$  over subtropical South America is reduced to about a half of its original value when the strongest cold surges are excluded. Similarly, exclusion of just 10% of the cold-surge days reduces the distinctive tongue of maximum meridional heat transport by transient eddies ( $\overline{T'v'_{925}}$ ) along the subtropical Andes by up to a factor 3 and virtually eliminates the meridional heat transport at latitudes lower than  $15^{\circ}\text{S}$  (Figs. A1c, d).

To assess the role of the cold surges upon the daily-to-weekly variability of low-level circulation and temperature during the rest of the year, Fig. A2 shows the annual march of the high-frequency (3–12-day period) standard deviation of SLP and  $T_{925}$  along  $60^{\circ}\text{W}$ . Throughout the year, the standard deviation of SLP to the east of the Andes between  $30^{\circ}$  and  $15^{\circ}\text{S}$  is well above the subtropical background level. Even at the height of the austral summer, high-frequency fluctuations of SLP over subtropical South America are quite pronounced and largely produced by the frequent passage of cold surges. Similar results emerge from the annual march of the standard deviation of  $T_{925}$ , although the late winter peak is more pronounced and the synoptic-scale variability during the austral summer is modest.

## REFERENCES

- Berbery, E. H., and C. S. Vera, 1996: Characteristics of the Southern Hemisphere winter storm track with filtered and unfiltered data. *J. Atmos. Sci.*, **53**, 468–481.
- Bosart, L. F., A. R. Lupo, D. J. Knight, E. G. Hoffman, and J. J. Nocera, 1998: Cyclonic and anticyclonic South American cold surges. Preprints, *Eighth Conf. on Mountain Meteorology*, Flagstaff, AZ, Amer. Meteor. Soc., 264–267.
- Boyle, J. S., and T. J. Chen, 1987: Synoptic aspects of the wintertime East Asian monsoon. *Monsoon Meteorology*, C. P. Chang and T. N. Krishnamurti, Eds., Oxford University Press, 125–160.
- Colle, B., and C. Mass, 1995: The structure and evolution of cold surges east of the Rocky Mountains. *Mon. Wea. Rev.*, **123**, 2577–2610.
- Compagnucci, R. H., and M. A. Salles, 1997: Surface pressure patterns during the year over southern South America. *Int. J. Climatol.*, **17**, 635–653.
- Fortune, M. A., and V. E. Kousky, 1983: Two severe freezes in Brazil: Precursors and synoptic evolution. *Mon. Wea. Rev.*, **111**, 181–196.
- Gan, M. A., and V. Rao, 1994: The influence of the Andes cordillera on transient disturbances. *Mon. Wea. Rev.*, **122**, 1141–1157.
- Garreaud, R. D., 1999: Cold air incursions over subtropical and tropical South America. A numerical case study. *Mon. Wea. Rev.*, **127**, 2823–2853.
- , and J. M. Wallace, 1998: Summertime incursions of midlatitude air into tropical and subtropical South America. *Mon. Wea. Rev.*, **126**, 2713–2733.
- Hamilton, M. G., and J. R. Tarifa, 1978: Synoptic aspects of a polar outbreak leading to frost in tropical Brazil, July 1972. *Mon. Wea. Rev.*, **106**, 1545–1556.

- Hastenrath, S., 1991: *Climate Dynamics of the Tropics*. 2d ed. Kluwer Academic, 488 pp.
- Kalnay, E., and Coauthors, 1996: The NCEP/NCAR 40-Year Reanalysis Project. *Bull. Amer. Meteor. Soc.*, **77**, 437–472.
- Kiladis, G. N., and K. M. Weickmann, 1997: Horizontal structure and seasonality of large-scale circulations associated with sub-monthly tropical convection. *Mon. Wea. Rev.*, **125**, 1997–2013.
- Knight, J. D., and L. F. Bosart, 1998: A modeling study of South American cold air damming and frontogenesis east of the Andes. Preprints, *Eighth Conf. on Mountain Meteorology*, Flagstaff, AZ, Amer. Meteor. Soc., 268–269.
- Kousky, V. E., 1979: Frontal influences on northeast Brazil. *Mon. Wea. Rev.*, **107**, 1140–1153.
- , and J. Ferreira, 1981: Frontal influences on northeast Brazil: Their spatial distributions, origins and effects. *Mon. Wea. Rev.*, **109**, 1999–2008.
- , and I. Cavalcanti, 1997: The principal modes of high-frequency variability over the South American region. Preprints, *Fifth Int. Conf. on Southern Hemisphere Meteorology and Oceanography*, Pretoria, South Africa, Amer. Meteor. Soc., 226–227.
- Krishnamurti, T. N., M. Tewari, D. R. Chakraborty, J. Marengo, P. L. Silva Dias, and P. Satyamurty, 1999: Downstream amplification: A possible precursor to major freeze events over southeastern Brazil. *Wea. Forecasting*, **14**, 242–270.
- Lau, K. M., and C. P. Chang, 1987: Planetary scale aspects of the winter monsoon and atmospheric teleconnection. *Monsoon Meteorology*, C. P. Chang and T. N. Krishnamurti, Eds., Oxford University Press, 161–202.
- Liebmann, B., and C. A. Smith, 1996: Description of a complete (interpolated) outgoing longwave radiation dataset. *Bull. Amer. Meteor. Soc.*, **77**, 1275–1277.
- , G. Kiladis, J. Marengo, T. Ambrizzi, and J. D. Glick, 1999: Submonthly convective variability over South America and the South Atlantic convergence zone. *J. Climate*, **12**, 1877–1891.
- Marengo, J., A. Cornejo, P. Satyamurty, C. Nobre, and W. Sea, 1997: Cold surges in tropical and extratropical South America: The strong event in June 1994. *Mon. Wea. Rev.*, **125**, 2759–2786.
- Montes de Oca, I., 1995: Geografía y Clima de Bolivia (Geography and climate of Bolivia). *Bull. Inst. Fr. Etud. Andines*, **24**, 357–368.
- Parmenter, F. C., 1976: A Southern Hemisphere cold front passage at the equator. *Bull. Amer. Meteor. Soc.*, **57**, 1435–1440.
- Pierrehumbert, R. T., and B. Wyman, 1985: Upstream effects of mesoscale mountains. *J. Atmos. Sci.*, **42**, 977–995.
- Ramage, C. S., 1971: *Monsoon Meteorology*. Academic Press, 359 pp.
- Ratisbona, C. R., 1976: The climate of Brazil. *Climate of Central and South America*, W. Schwerdtfeger and H. E. Landsberg, Eds., World Survey of Climatology, Vol. 12, Elsevier, 219–293.
- Riehl, H., 1954: *Tropical Meteorology*. McGraw-Hill, 392 pp.
- Schultz, D. M., W. E. Bracken, L. F. Bosart, G. J. Hakim, M. A. Bedrick, M. J. Dickinson, and K. R. Tyle, 1997: The 1993 Superstorm cold surge: Frontal structure, gap flow, and tropical impact. *Mon. Wea. Rev.*, **125**, 5–39.
- , —, and —, 1998: Planetary- and synoptic-scale signatures associated with Central American cold surges. *Mon. Wea. Rev.*, **126**, 5–27.
- Seluchi, M., Y. V. Serafini, and H. Le Treut, 1998: The impact of the Andes on transient atmospheric systems: A comparison between observations and GCM results. *Mon. Wea. Rev.*, **126**, 895–912.
- Slingo, J. M., 1998: Extratropical forcing of tropical convection in a northern winter simulation with the UGAMP GCM. *Quart. J. R. Meteor. Soc.*, **124**, 27–52.
- Uccellini, L. W., and D. R. Johnson, 1979: The coupling of upper and lower tropospheric jet streaks and implications in development of severe convective storms. *Mon. Wea. Rev.*, **107**, 682–703.
- Vera, C. S., and P. K. Vigliarolo, 2000: A diagnostic study of cold-air outbreaks over South America. *Mon. Wea. Rev.*, **128**, 3–24.
- Wu, M. C., and J. C. L. Chan, 1995: Surface features of winter monsoon surges over South China. *Mon. Wea. Rev.*, **123**, 662–680.
- , and —, 1997: Upper-level features associated with winter monsoon surges over South China. *Mon. Wea. Rev.*, **125**, 317–340.
- Xu, Q., 1985: A theoretical study of cold air damming. *J. Atmos. Sci.*, **47**, 2969–2985.